Interplay of Segmental and Normal Mode Dynamics in Polymer Networks Undergoing Chemical Cross-Linking. Epoxy/ Amine-Terminated Linear and Star PPO Formulations

Jovan Mijović,* Yuefeng Han, Mingyun Sun, and Srdjan Pejanović†

Department of Chemical Engineering and Chemistry and The Herman F. Mark Polymer Research Institute, Polytechnic University, Six Metrotech Center, Brooklyn, New York 11201

Received January 28, 2003; Revised Manuscript Received April 8, 2003

ABSTRACT: An investigation was conducted of segmental and normal mode dynamics during cross-linking of reactive systems where one of the components exhibits, in addition to the transverse dipole moment ($\mu^{\perp}$) component that gives rise to the segmental α process, a persistent cumulative dipole moment ($\mu^{\parallel}$) along the chain contour that can be relaxed via the normal mode process. The systems studied were composed of an amine-terminated linear or three-arm star poly(propylene oxide), which contains both $\mu^{\perp}$ and $\mu^{\parallel}$, and a bifunctional epoxy prepolymer. The kinetics of network formation were evaluated by Fourier transform near-infrared spectroscopy (NIR), and the dynamics were investigated by broad-band dielectric relaxation spectroscopy (DRS) and dynamic mechanical spectroscopy (DMS). The dynamics of networks containing linear and star chains were similar but not identical. The average relaxation time for segmental (τ_S) and normal mode (τ_N) increases in the course of network formation, but the distance between τ_S and τ_N varies little and the T_g-scaled fragility remains unchanged. The spectra become thermodielectrically complex following the onset of reactions and broaden in the course of cure. Segmental and normal mode relaxations overlap increasingly during cure but, interestingly, retain their identities. There is a decrease in the dielectric relaxation strength for the segmental process ($\Delta\epsilon_S$) and a simultaneous (unexpected) increase in the dielectric relaxation strength for the normal mode process ($\Delta\epsilon_N$). Before gelation, the DMS response was characterized by segmental and terminal relaxation zone. The gel point was observed at a conversion above that predicted by the gelation theory, and an explanation was put forward.

Introduction

The segmental dynamics (the α process) of polymer networks that undergo temporal evolution of structure as a result of chemical cross-linking have been investigated by several groups,[1−22] including our own.[23−28] This work adds a new dimension to the past efforts by examining the dynamics of reactive network-forming systems where one of the components exhibits, in addition to the transverse dipole moment component ($\mu^{\perp}$) that gives rise to the segmental α process, a persistent cumulative dipole moment along the chain contour ($\mu^{\parallel}$). This part of dipole moment of the polymer molecule is present when the repeat unit lacks a plane of symmetry perpendicular to the chain contour, and it can be relaxed via the normal mode process,[29] termed α_N. Moreover, for a sequence of such uninverted units, the dipole vector must correlate with the directional vector, affording a comparison of dielectric and viscoelastic relaxations. How the chemorheology that underlies gelation and vitrification in cross-linking networks affects segmental and normal mode dynamics is a fundamentally important and incompletely understood problem.

The presence of two dielectric dispersions, α and α_N, was first reported in the pioneering studies by Stockmayer and co-workers,[30−33] who termed chain molecules with a dipole component *parallel* to the chain contour *type A*. A dipole component *perpendicular* to the main chain is termed *type B*. Following Stockmayer's seminal work, a number of investigations of the dynamics of type A homopolymers, copolymers, polymer blends, and star polymers in solution and bulk have been reported,[34−56] and several excellent reviews of this subject have been published.[57−60] However, nearly all of those studies have been concerned with time-invariant systems; there are no reports in the literature of a systematic study of the simultaneous change in the segmental *and* normal mode dynamics in networks undergoing chemical cross-linking.

Therefore, the objective of this work is to provide an insight into the fundamental features *of* and the interplay *between* the segmental and the normal mode dynamics during network formation in the systems where one reactive component is a type A polymer.

The systems studied were composed of an end-functionalized poly(propylene oxide) that contains type A and B dipoles and a bifunctional epoxy prepolymer. Two different architectures of poly(propylene oxide) chains were investigated: (1) *linear* chains (hereafter referred to as PPO) with symmetrical dipole inversion and (2) *three-arm star-shaped* chains (hereafter referred to as SPPO) with each arm emanating from a central branching point and containing an uninverted dipole sequence. A comprehensive investigation of the segmental and normal mode dynamics of the *neat* PPOs and SPPOs has been recently reported by our group.[61]

Experimental Section

Materials. The two-component reactive mixtures investigated were composed of DGEBA (diglycidyl ether of bisphenol A), molecular weight of 374 g/mol (Aldrich), and a primary amine end-terminated linear (PPO) or star (SPPO) (poly(propylene oxide). The two PPOs used (Huntsman) had molecular weight of 2000 g/mol (PPO2000) and 4000 g/mol (PPO4000), the polydispersity index < 1.1, and were characterized by symmetrical dipole inversion. The two SPPOs used

† Faculty of Technology, University of Belgrade, Belgrade, Serbia.

* To whom correspondence should be addressed. E-mail jmijovic@poly.edu.

10.1021/ma030072l CCC: $25.00
Published on Web 05/20/2003

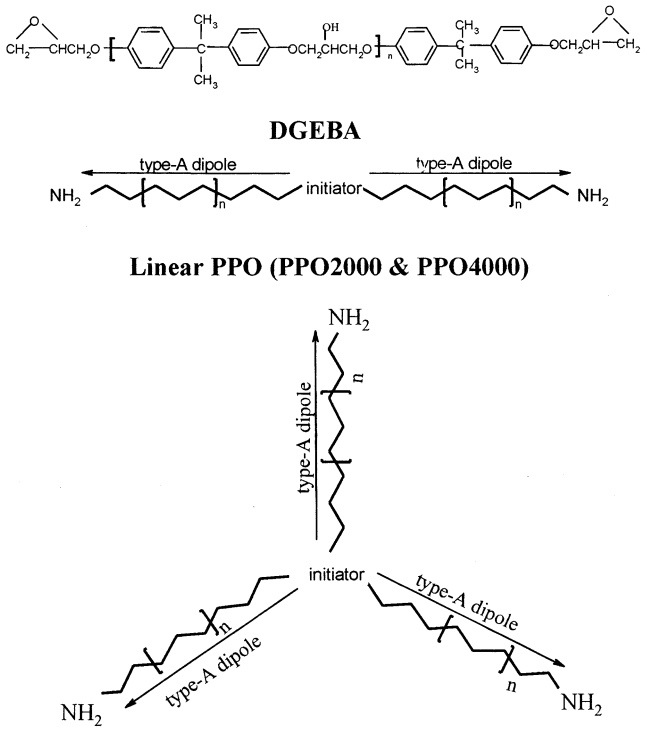

Figure 1. Chemical structure of DGEBA, linear poly(propylene oxide) (PPO), and three-arm star poly(propylene oxide) (SPPO).

(Huntsman) had molecular weight of 3000 g/mol (SPPO3000) and 5000 g/mol (SPPO5000), the polydispersity index < 1.1, and were characterized by three arms, each emanating from a central branching point and containing an uninverted dipole sequence. The neat PPOs (PPO2000 and PPO4000) had a DSC T_g of −67 °C; the neat SPPOs (SPPO3000 and SPPO5000) had a DSC T_g of −65 °C.

The chemical structures of the reactive components are shown in Figure 1. The two components were mixed in the stoichiometric ratio, and the mixture was degassed prior to curing. The mixtures of DGEBA with PPO2000 and PPO4000 are referred to as MPPO2000 and MPPO4000, respectively. The mixtures of DGEBA with SPPO3000 and SPPO5000 are referred to as MSPPO3000 and MSPPO5000, respectively. The sample codes are summarized in Table 1. The chemical changes during isothermal heating of the reactive mixture were monitored by Fourier transform near-infrared (NIR) spectroscopy.

Techniques. *Dielectric Relaxation Spectroscopy* (*DRS*). Our facility combines commercial and custom-made instruments that include (1) Novocontrol's α high-resolution dielectric analyzer (3 μHz−10 MHz), (2) Solartron 1260 impedance/gain phase analyzer (10 μHz−32 MHz), (3) Hewlett-Packard 4284A precision LCR meter (20 Hz−1 MHz), (4) Hewlett-Packard 8752A network analyzer (300 kHz−1.3 GHz), and (5) Hewlett-Packard 4291B RF impedance analyzer (1 MHz−1.8 GHz). All instruments are interfaced to computers and equipped with heating/cooling controls, including Novocontrol's Novocool system custom-modified for measurements over the entire frequency range from 3 μHz to 1.8 GHz. Further details of our DRS facility are given elsewhere.[62,63]

Dynamic Mechanical Spectroscopy (*DMS*). Experiments were conducted using a Rheometric Scientific's Advanced Rheometric Expansion System (ARES) rheometer. Measurements were performed in the frequency range from 0.01 to 100 rad/s and the temperature range from 213 to 293 K. A parallel plate configuration (d = 8 mm and d = 25 mm) was employed with a typical gap between the plates of ca. 1.2−2.0 mm. Strain values were adjusted from 0.2 to 25% for a measurable torque in the linear viscoelastic range, and linearity was verified by strain sweeps.

Differential Scanning Calorimetry (*DSC*). The glass transition temperature was determined by DSC. The samples were first cooled at 20 K/min and then heated at 10 K/min; the T_g was read from the midpoint of the heating trace. A TA Instruments Co. DSC model 2920 was used.

Fourier Transform Infrared Spectroscopy (*FTIR*). FTIR spectroscopy was performed using a Nicolet Magna-IR system 750 spectrometer with spectral range coverage from 15 800 to 50 cm^{-1} and the Vectra interferometer with better than 0.1 cm^{-1} resolution. Near-infrared (NIR) data were obtained using a calcium fluoride beam splitter, a white light source, and a mercury−cadmium−tellurium (MCT) detector. A silica type optical fiber was used for in-situ monitoring of reactions in the remote mode. The details of our use of the technique may be found elsewhere.[64] The extent of reaction of epoxide groups is calculated by comparison of the area under the epoxide peak at a given reaction time to the initial peak area and normalizing with respect to a group peak that is not involved in the reaction.

Molecular Simulation (MS). Commercial software, Materials Studio (Accelrys Inc.), was used in the simulation study. An amorphous cell was constructed with the Amorphous Cell Module, and the interatomic interactions were modeled using the COMPASS field force. A density of 1 and 1.07 g/cm^3 was used for the stoichiometric mixture and the cured network, respectively. Upon completion of minimization, the amorphous cell was equilibrated at 298 K for 20 ps. Constant temperature, constant density condition (NVT ensemble) was used in studying the structure, and further details are provided elsewhere.[65]

Results and Discussion

Individual Components: PPO and DGEBA. We preface the discussion of our dielectric results by pointing out that the fundamental aspects of DRS, theoretical and experimental, are well established and will not be discussed here; the interested reader is referred to a number of excellent books and key reviews.[66−68] The relaxation behavior of PPOs and SPPOs is similar but not identical; some interesting differences were observed and are highlighted below. Dielectric loss in the fre-

Table 1. Sample Descriptions and Codes

description	MW (g/mol)	functionality	code
linear poly(propylene oxide)	380	4	PPO380
linear poly(propylene oxide)	640	4	PPO640
linear poly(propylene oxide)	2000	4	PPO2000
linear poly(propylene oxide)	4000	4	PPO4000
three arm star-shaped poly(propylene oxide)	3000	6	SPPO3000
three arm star-shaped poly(propylene oxide)	5000	6	SPPO5000
diglycidyl ether of bisphenol A	374	2	DGEBA
stoichiometric mixture: PPO2000 + DGEBA			MPPO2000
stoichiometric mixture: PPO4000 + DGEBA			MPPO4000
stoichiometric mixture: SPPO3000 + DGEBA			MSPPO3000
stoichiometric mixture: SPPO5000 + DGEBA			MSPPO5000

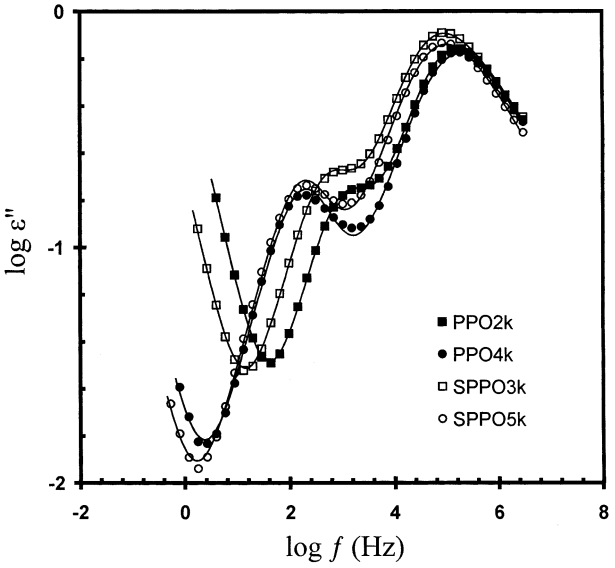

Figure 2. Dielectric loss in the frequency domain for two PPOs and two SPPOs at 243 K, with molecular weight as a parameter.

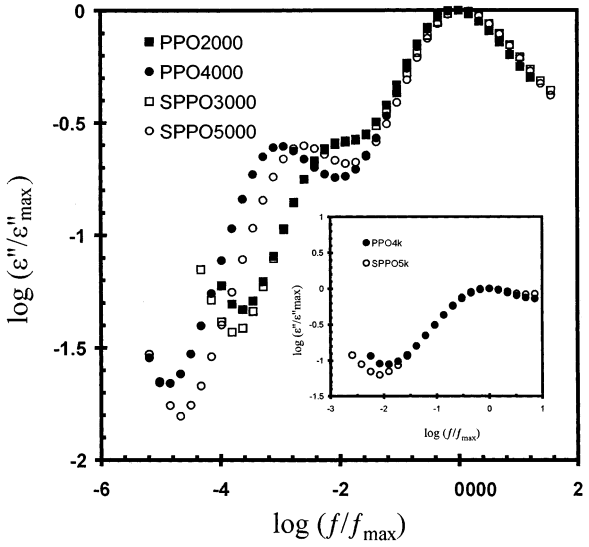

Figure 3. Normalized dielectric loss in the frequency domain for two PPOs and two SPPOs with molecular weight as a parameter. Inset: normalized normal mode distribution for PPO4000 and SPPO5000.

quency domain at 243 K for two PPOs and two SPPOs is shown in Figure 2. The segmental and the normal mode process are clearly visible; their interplay in the neat PPOs and SPPOs (with molecular weight ranging from 2000 to 12 000 g/mol) has been discussed in our recent communication[61] and will not be revisited here. However, briefly, the solid lines in Figure 2 are fits to the Havriliak−Negami (HN) equation[69] for the case of the segmental process and the Cole−Cole (CC) equation[70] for the normal mode process. Both relaxations in PPOs and SPPOs are thermodielectrically simple with the Kohlrausch−Williams−Watts[71] (KWW) β parameter of 0.54 and 0.60, respectively. Also, both processes show a well-known Vogel−Fulcher−Tammann (VFT) temperature dependence of the relaxation time. An examination of the segmental process reveals no effect of the molecular weight of PPO or SPPO on the average relaxation time, τ_S. The effect of architecture (linear vs star) on the average relaxation time for the segmental process, however, is small but noticeable; $\tau_S \approx 2$ and 4 μs for PPO and SPPO, respectively.

We note that only even normal modes are dielectrically active in the samples with symmetrical dipole inversion and that the contribution from the second normal mode dominates the response (i.e., $\tau_N \cong \tau_{N2}$). Also, the dielectric response of our PPOs/SPPOs reflects the normal mode process associated with M_a—the molecular weight of the arm that contains the uninverted dipole sequence. An interesting question is whether the average relaxation time for the normal mode (τ_N) differs in PPO and SPPO with the same length of the uninverted dipole sequence (M_a). That condition is met for PPO2000 and SPPO3000, both of which have the arm length of $M_a = 1000$ g/mol. We observe τ_N of 3×10^{-4} s for SPPO3000 and 1.4×10^{-4} s for PPO2000. Again, the difference is small but noticeable, and we conclude that the architecture of the polymer chain does play a role in the normal mode process as well. In our earlier study of neat PPOs/SPPOs[61] we reported no change in τ_N for diols (PPO) and triols (SPPO) having the same arm length. After careful reexamination of those data, however, we find that the relaxation times for normal and segmental modes of triols (MW = 3000 and 6000 g/mol) are slightly above those for the corresponding diols (ref 61, Figure 3).

Another insight into the difference between PPOs and SPPOs is obtained from the normalized spectra presented in Figure 3. Normalization with respect to the segmental process brings out the dependence of τ_N on molecular weight and architecture. Note how the spectra of PPO2000 and SPPO3000 overlap completely, which is expected considering the equal arm length in these two systems ($M_a = 1000$ g/mol). With an increasing arm length (PPO2000 = SPPO3000 < SPPO5000 < PPO4000), the normal mode slows down and progressively separates out from the segmental mode. It is also interesting to note that the spectral shape of PPO vs SPPO is not affected by molecular weight or architecture for either normal or segmental mode. For example, normalized normal mode spectra of PPO4000 and SPPO5000 coincide, as illustrated in the inset in Figure 3. The observed independence of the spectral shape for the normal mode process on the molecular weight below M_e is in agreement with the previous findings by Watanabe.[59]

Dielectric loss in the frequency domain for DGEBA is shown in Figure 4. The segmental (α) and the local (β) process are evident: note how the α process evolves to longer relaxation times with decreasing temperature.[72] The α process in DGEBA is also thermodielectrically simple with a KWW β parameter of 0.56. Thermodielectric simplicity and a somewhat lower KWW β parameter were recently reported for higher molecular weight DGEBA.[73]

Mixtures of PPO and DGEBA Prior to the Onset of Chemical Reaction. We start by restating that the stoichiometric mixtures of DGEBA with PPOs and/or SPPOs are coded by placing a letter M before PPO and/or SPPO, as detailed in Table 1. In sum, four type A network-forming formulations were studied: MPPO2000, MPPO4000, MSPPO3000, and MSPPO5000. In Figure 5, we present a dielectric spectrum of MPPO4000 with temperature as a parameter *before* the onset of reaction. Similar spectra were obtained for other mixtures, though a greater overlap between normal and segmental modes was observed in MPPO2000 and MSPPO3000

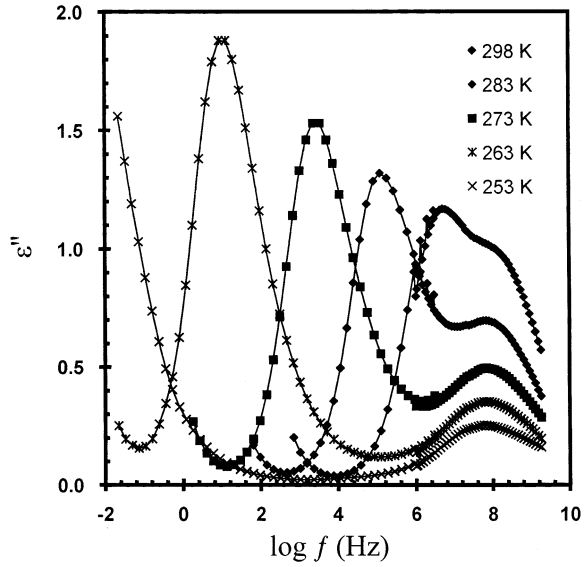

Figure 4. Dielectric loss in the frequency domain for DGEBA with temperature as a parameter.

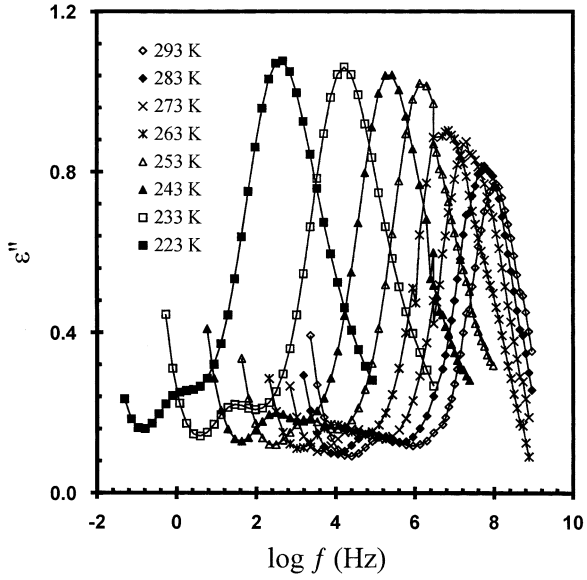

Figure 5. Dielectric loss in the frequency domain for MPPO4000 with temperature as a parameter prior to the onset of reaction.

because of the lower molecular weight of PPO/SPPO in those mixtures. Note that the normal mode process in MPPO4000 and MSPPO5000 remains active and well separated from the segmental process. We reiterate that the normal mode process in the mixture is contributed by PPO or SPPO, i.e., the type A component with a cumulative dipole moment along the chain contour. The segmental process in the mixture encompasses segmental processes in DGEBA and PPO. A single dielectric dispersion (and a single calorimetric T_g) that characterizes the segmental process in the mixture is a signature of miscibility, at least at the length scale of the DRS measurement. The α dynamics of all unreacted mixtures are also characterized by thermodielectric simplicity and a spectrum slightly broader than that of either individual component (KWW β parameter of 0.48 was obtained). Interestingly, a broadening of the normal mode spectrum was also observed, and a best-fit KWW β parameter of 0.53 was recorded.

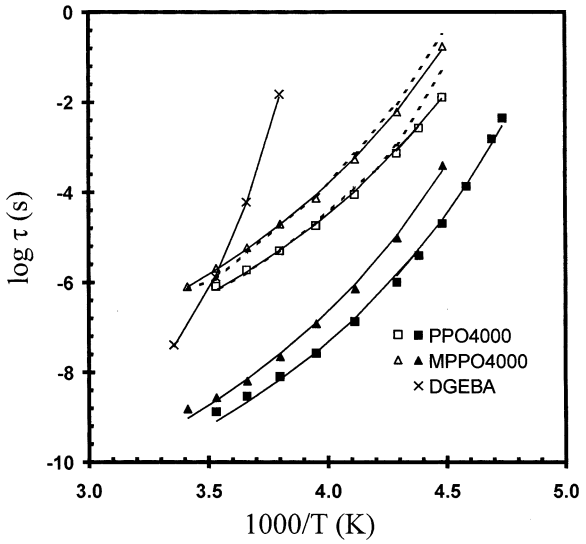

Figure 6. Average relaxation time as a function of reciprocal temperature for the individual components (DGEBA and PPO4000) and their mixture (MPPO4000) prior to the onset of reaction. Open symbols denote the normal mode process and filled symbols the segmental process. Dashed lines are the prediction of the Rouse model.

Table 2. VFT Parameters for DGEBA, PPO4000, and MPPO4000

material	τ_0 (s)	$B(k)$	T_v (K)
DGEBA	1.0×10^{-14}	1148	222
PPO4000	1.0×10^{-14}	1420	157
MPPO4000	1.0×10^{-14}	1525	159

The temperature dependence of the average relaxation time for segmental (τ_S) and normal mode (τ_N) for the unreacted mixture was examined next. The results for MPPOs are presented first (Figure 6), and the data for the neat PPO 4000 are included for completion. The solid lines in Figure 6 are fits to the VFT functional form. The segmental process in the mixture is contributed largely by PPO and, consequently, has fit parameters similar to those for the neat PPO, as shown in Table 2. The dashed lines in Figure 6 represent the prediction of the Rouse model for the normal mode process based on the measured value of zero shear viscosity (or obtained by calculating $\eta_0 = \lim\{G''(\omega)/\omega\}$ as $\omega \rightarrow 0$). The excellent agreement between the measured relaxation time for the normal mode and the prediction of the Rouse model suggests that the relaxation mechanism in the mixture is the same as in the neat PPO. The observed increase in the average relaxation time (τ_N) at a given temperature is accounted for by the difference in the zero shear viscosity between the neat PPO and the mixture. A few interesting observations were made by contrasting the dynamics of PPO2000 and MPPO2000 with those of PPO4000 and MPPO4000. As expected, PPO2000 has the same τ_S as PPO4000. However, MPPO2000 has higher τ_S than MPPO4000 because of a higher relative concentration of DGEBA (higher T_g component) but a lower τ_N because of the lower molecular weight (2K vs 4K). The T_g*-scaled fragility plot[74] for the segmental process (not shown here) reveals no difference between the neat PPOs and their unreacted mixtures with DGEBA; the neat DGEBA itself is a more fragile glass-former. It is also interesting to note that MPPO2000 and MPPO4000 have identical fragilities despite the difference in the relative concentration of DGEBA in these mixtures.

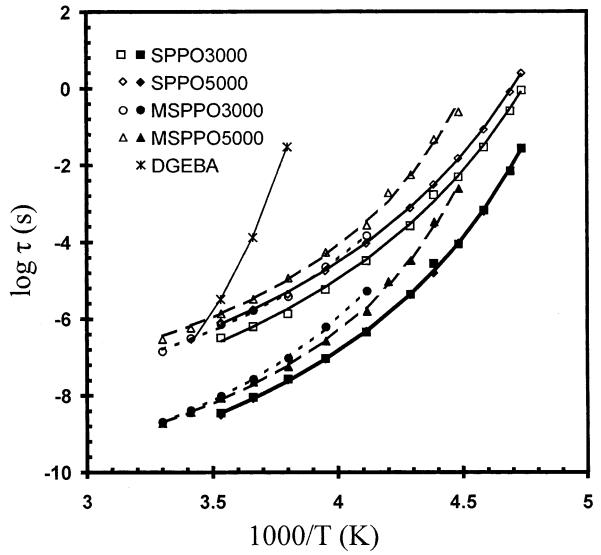

Figure 7. Average relaxation time as a function of reciprocal temperature for the individual components (DGEBA and SPPO5000) and their mixture (MSPPO5000) prior to the onset of reaction. Open symbols denote the normal mode process and filled symbols the segmental process.

Both normal and segmental modes are also discerned in the neat SPPOs and in the MSPPOs. The loss spectra exhibit a shift to lower frequency upon the addition of a higher T_g component DGEBA; the greater weight fraction of DGEBA causes a more pronounced shift in MSPPO3000 than MSPPO5000. The segmental process for all samples is well described by the HN functional form. The best results for the normal mode process are obtained with the CC functional form. The temperature dependence of the average relaxation time for segmental (τ_S) and normal (τ_N) mode (obtained from HN and CC fits) in the neat SPPOs and in MSPPOs was examined next, and those results are plotted in Figure 7. Filled and open symbols represent the segmental and the normal mode process, respectively, and solid lines are best fits to the VFT equation. An increase in the molecular weight slows down the normal mode but has no effect on the segmental mode of the neat SPPOs. The addition of DGEBA to SPPO slows down the segmental process. The T_g*-scaled fragility plot (not shown here), where T_g* is the operational value of the dielectric glass transition temperature that corresponds to $\tau_S = 100$ s, reveals that (1) the fragility of SPPO does not vary with molecular weight and (2) the fragility of MSPPO lies between the values for the individual components, SPPO and DGEBA. The fragility index[75] (FI) for SPPO and DGEBA was 0.68 and 0.76, respectively, and the rule of mixtures was utilized to calculate the FI of the mixtures. Fragility can be quantified in various ways; we used the $F_{1/2}$ notation, where $F_{1/2} = 2T_g/T_{1/2} - 1$ and $\tau(T_{1/2}) = 10^6$ s.[76] The calculated $F_{1/2}$ for MSPPO3000 and MSPPO5000 was 0.70 and 0.69, respectively, in excellent agreement with the value 0.70, extracted from the data. It is intriguing that MSPPO3000 and MSPPO5000 have identical fragility despite the difference in the relative concentration of DGEBA in these two systems.

Mixtures of PPO and DGEBA during Chemical Reaction. We now turn attention to the effect of cross-linking on dynamics. Note that we use the term "cross-linking" in a broad sense to describe the advancement of reaction. What we actually measure, however, is conversion and not the degree of cross-linking; these two terms are related but not the same. The chemical changes during isothermal heating of the reactive mixture were monitored with near-infrared (NIR) spectroscopy by following the disappearance of epoxy and amine groups and the formation of hydroxyl groups. An example of a series of NIR spectra generated during cure of MPPO4000 is presented in Figure 8. Curing was conducted at 100 °C for MPPO2000, 130 °C for MPPO4000, 100 °C for MSPPO3000, and 132 °C for MSPPO5000. All characteristic absorption peaks present in epoxy−amine systems were evident.[77] The extent of reaction of epoxide groups (i.e., conversion) is calculated by comparison of the area under the epoxide peak at a given reaction time to the initial peak area and normalized with respect to a group peak (the aromatic C−H stretch at 4622 cm^{-1}, in this case) that is not involved in the reaction. The extent of reaction was expressed as a function of reaction time, and the corresponding kinetics were used throughout this study. The DSC $T_{g\infty}$ for the fully cured network was −43 °C for MPPO2000, −56 °C for MPPO4000, −48 °C for MSPPO3000, and −59 °C for MSPPO5000 (neat PPOs and SPPOs have a DSC T_g of −67 and −65 °C, respectively).

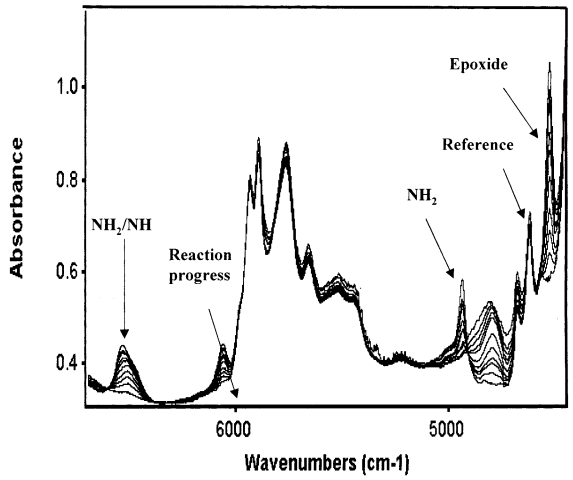

Figure 8. A series of NIR spectra obtained at various times during cure of MPPO4000.

Dielectric loss in the frequency domain for a fully cured MPPO4000 network with temperature as a parameter is shown in Figure 9. We examine the fully cured network first to accentuate the difference with the unreacted mixture, shown in Figure 5. Three salient points regarding the spectra of Figure 9 are as follows. First, the maximum value of dielectric loss (ϵ''_{max}) decreases with decreasing temperature, in contrast to the trend observed in the unreacted MPPO4000 (Figure 5), even though the segmental relaxation strength ($\Delta\epsilon_s$) increases with decreasing temperature in both cases. Second, the spectra of unreacted mixtures are initially thermodielectrically simple but turn complex shortly after the reactions begin. And third, the normal mode process remains active at all stages of cure, including the fully cured network, despite a notable change in the shape of the overall spectrum. We shall amplify on those observations later in the text. The solid lines in Figure 9 represent a combined fit to the HN equation for the segmental process and the CC equation for the normal mode. Fully cured MPPO2000 (not shown here) also shows both segmental and normal modes, with a more pronounced overlap between these two modes. We shall now illustrate and quantify the difference in the dielec-

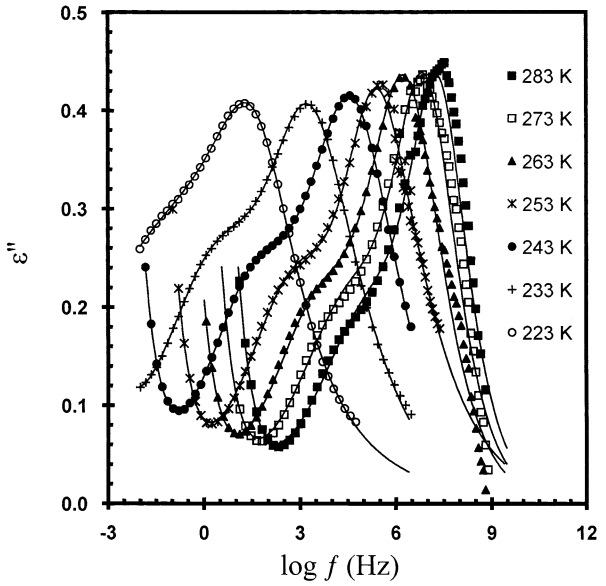

Figure 9. Dielectric loss in the frequency domain for fully cured MPPO4000 with temperature as a parameter.

tric spectra of MPPOs and MSPPOs as a function of extent of reaction and temperature.

Of interest is to understand how (and if) the segmental and the normal mode process interact in the course of network formation and, to that end, a series of partially cured networks at different extent of cross-linking were prepared and tested. As previously stated, the extent of reaction of each network was determined from the kinetic data. The DRS results are exemplified in Figures 10 and 11. Figure 10 shows dielectric permittivity (A) and dielectric loss (B) in the frequency domain with extent of reaction as a parameter for MPPO4000. Figure 11 shows dielectric loss in the frequency domain with extent of reaction as a parameter for MSPPO5000. Note the systematic decrease (Figure 10A) in the limiting low-frequency permittivity (ϵ'_0) and the maximum value of the loss (ϵ''_{max}) and the concomitant increase in the average relaxation time (shift to lower frequency) of both relaxation modes. In what follows we shall build our discussion of changing dynamics around the dependence on temperature and degree of cross-linking of the key dynamic parameters that include the dielectric relaxation strength, the average relaxation time, and the relaxation spectrum.

Changes in Relaxation Strength during Network Formation. We start by considering the effect of extent of reaction on relaxation strength ($\Delta\epsilon$), an important materials characteristic that depends on the chemical structure and molecular architecture. The relaxation strength of a process is defined as $\Delta\epsilon = \epsilon'_0 - \epsilon'_\infty$, where ϵ'_0 and ϵ'_∞ represent the limiting low- and high-frequency dielectric permittivity, respectively, for a particular process (segmental or normal mode) and is proportional to the concentration of dipoles and the mean-squared dipole moment per molecule. The dielectric relaxation strengths for the segmental mode ($\Delta\epsilon_S$) and the normal mode ($\Delta\epsilon_N$) were calculated from the fits of data and are shown in Figure 12. In the course of cure we observe a decrease in $\Delta\epsilon_S$ of about 55% in MPPO4000 and 50% in MSPPO5000 and an increase in $\Delta\epsilon_N$ of about 150% in MPPO4000 and 113% in MSPPO5000. The observed decrease in the limiting low-frequency dielectric permittivity (ϵ'_0) with increasing

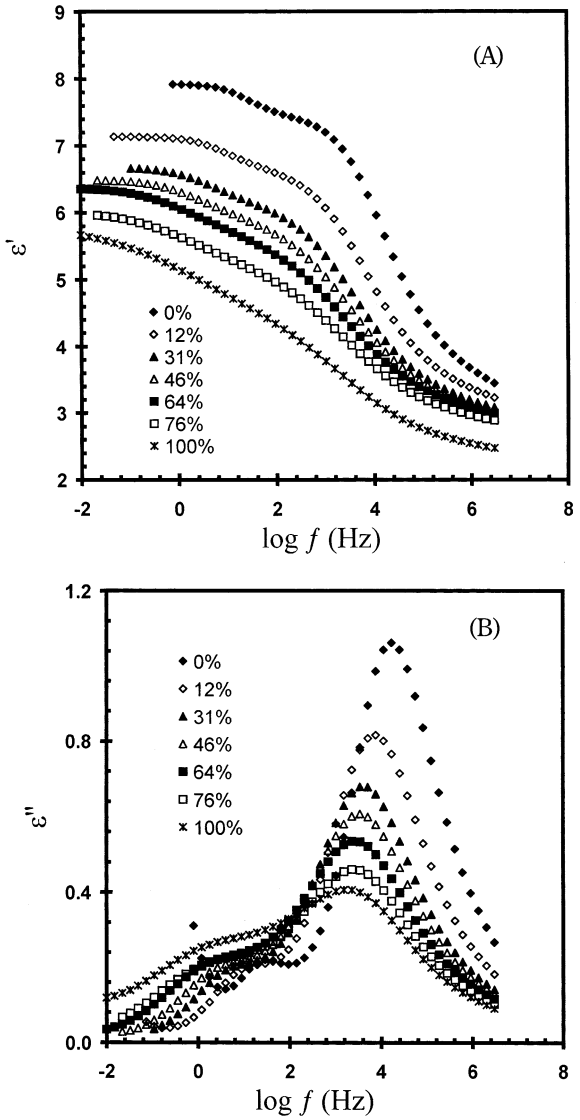

Figure 10. Dielectric permittivity (A) and loss (B) for MPPO4000 in the frequency domain with extent of reaction as a parameter.

extent of reaction, which drives the decrease in $\Delta\epsilon_S$, is a direct consequence of the changing nature of the segmental process, reflecting a diminishing ability of dipolar moieties to store the electric field. Specifically, the decrease in $\Delta\epsilon_S$ with increasing extent of reaction is attributed to the changes in the physical architecture (topology) of the network caused by cross-linking and the chemical nature of the dipole unit. (Epoxy and primary amine groups are replaced by lesser dipole strength tertiary amine and hydroxyl groups, the latter being at the origin of the localized β process.) Deconvolution of normal and segmental processes in MPPO2000 was less reliable because of a more pronounced overlap between these two modes. Next, an attempt was made to quantify $\Delta\epsilon_S$. Following Williams,[21,78] the segmental relaxation strength could be represented as

$$\Delta\epsilon_S(\alpha) = F(\epsilon_0,\epsilon_\infty)\sum_i c_i(\alpha)\mu_i^2 \qquad (1)$$

where $F(\epsilon_0,\epsilon_\infty)$ is a function of limiting permittivities; c_i is the concentration of species i with a dipole moment

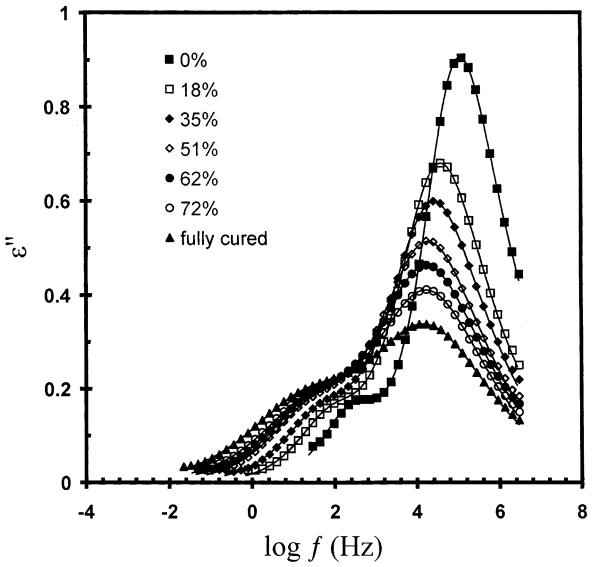

Figure 11. Dielectric loss for MSPPO5000 in the frequency domain with extent of reaction as a parameter.

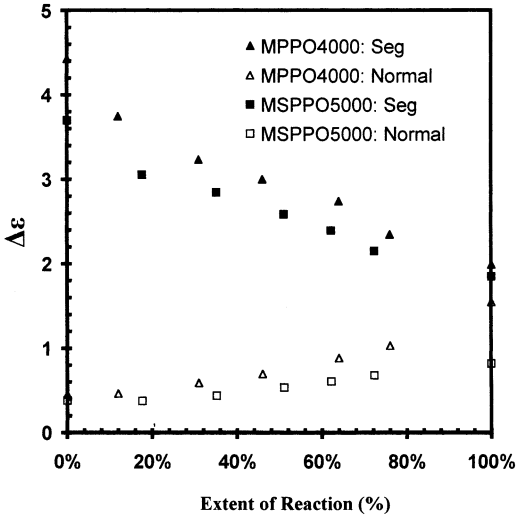

Figure 12. Dielectric relaxation strength for the segmental ($\Delta\epsilon_S$) and normal mode ($\Delta\epsilon_N$) process in MPPO4000 and MSPPO5000 as a function of extent of reaction.

μ_i, at a conversion α_i (%). For a polymer system[21,79] we write

$$F(\epsilon_0,\epsilon_\infty) = \frac{3\epsilon_0}{2\epsilon_0+\epsilon_\infty}\frac{4\pi N_A}{3kT}\left(\frac{\epsilon_\infty+2}{3}\right)^2 g \qquad (2)$$

where N_A is the Avogadro number, k is the Boltzmann constant, and g is the orientation correlation function of dipoles. We acknowledge that the general form of eq 2 was originally proposed for the static case[80] and for a system of homogeneous dipoles, but we employ it nonetheless as a useful tool for comparing the calculated and predicted values of the relaxation strength. Dipole moments of all groups that partake in our networks at different stages of network formation are listed in Table 3.[81] The concentration of each respective dipole and, consequently, the term $\sum_i c_i(\alpha)\mu_i^2$, are functions of conversion. A mechanistic study of reaction kinetics was beyond the scope of this work, and the actual situation was further simplified by neglecting the dipolar contribution of secondary amine. The results of our calculations for MPPO4000 and MSPPO5000 are summarized in Table 4. We observe that the term $\sum_i c_i(\alpha)\mu_i^2$ and the orientation correlation function (g) decrease with the advancement of cross-linking; for example, in MPPO4000 these two terms decrease by roughly 4% and 53%, respectively. The deviation of g from unity is a signature of correlation between dipoles. The decrease in g with conversion indicates increasing dipole correlation during cross-linking and represents a major factor that contributes to the observed decrease of the segmental relaxation strength. In MSPPO3000, g decreases from 0.67 to 0.35, indicating a greater overall increase in the correlation between dipoles than in MSPPO5000, where g decreases from 0.60 to 0.40.

Table 3. Dipole Moments (in D) of Groups Present during Network Formation

primary amine	ether (PPO)	epoxy	ether (DGEBA)	tertiary amine	secondary amine	hydroxyl
1.22	1.17	1.89	1.3	0.64	1.02	1.7

Table 4. Orientation Correlation Function of Dipoles as a Function of Degree of Cross-Linking

extent of reaction	$\sum_i c_i(t)\mu_i^2$ (mol D^2/L)	$\Delta\epsilon_S$	ϵ_0	ϵ_∞	g
MPPO4000: 0%	26.0	4.43	7.49	3.06	0.61
MPPO4000: 12%	25.9	3.75	6.69	2.94	0.55
MPPO4000: 31%	25.7	3.23	6.11	2.87	0.50
MPPO4000: 46%	25.5	3	5.83	2.83	0.48
MPPO4000: 64%	25.4	2.74	5.53	2.79	0.45
MPPO4000: 76%	25.2	2.35	5.04	2.70	0.41
MPPO4000: 100%	25.0	1.99	4.3	2.31	0.42
MSPPO5000: 0%	26.4	4.88	8.36	3.48	0.60
MSPPO5000: 18%	26.2	4.03	7.49	3.45	0.51
MSPPO5000: 35%	26	3.76	7.16	3.41	0.49
MSPPO5000: 51%	25.8	3.41	6.77	3.36	0.46
MSPPO5000: 62%	25.7	3.16	6.48	3.32	0.44
MSPPO5000: 72%	25.5	2.93	6.14	3.21	0.43
MSPPO5000: 100%	25.2	2.51	5.52	3.02	0.40

An interesting question is whether the observed decrease in g in the networks containing DGEBA as a spacer would differ if PPO were used as a spacer instead. To address that query, an experiment was carried out in which DGEBA (MW = 374 g/mol) was replaced with an epoxy-terminated PPO of approximately the same molecular weight (MW = 380 g/mol, coded PPO380). That results in a system where both components (epoxy-terminated and amine-terminated) have the *same* chemical structure of the main chain. The entire experimental sequence was repeated for this new system, and several interesting observations were made. First, the calculated value of g for the mixture of SPPO3000 and PPO380 decreased during cure from 0.70 to 0.49. Second, the overall decrease in g (0.20 for SPPO5000 and DGEBA; 0.21 for SPPO5000 and PPO380) was almost the same, indicating an identical increase in dipole correlation during cross-linking. And third, the lower value of g (0.60 in SPPO5000 and DGEBA vs 0.70 in SPPO5000 and PPO380) suggests that a more heterogeneous chemical structure may contribute to an increase in the correlation between dipole moieties. This is curious and represents an interesting subject for future study.

Next, we consider the relaxation strength of the normal mode process ($\Delta\epsilon_N$). Of particular interest here is the observed increase in $\Delta\epsilon_N$ during cross-linking. $\Delta\epsilon_N$ is related to the mean-squared end-to-end distance for a homopolymer with a narrow molecular weight distri-

bution according to the following equation:[57]

$$\Delta\epsilon_N = \frac{4\pi\rho N_A \mu^2}{3kT}\frac{\langle r^2\rangle}{M}F \qquad (3)$$

where μ is the cumulative type A dipole moment along the polymer (PPO or SPPO) chains, F is the ratio of the internal to external field and was chosen as unity, $\langle r^2\rangle$ is the mean-squared end-to-end distance, M is the molecular weight of the arm with uninverted dipole sequence in the PPO chain, and other symbols are as previously defined. An examination of eq 3 reveals that only two parameters change during isothermal cure: the network density, ρ, and the mean-squared end-to-end distance, $\langle r^2\rangle$. On the basis of the reported measurements of density of epoxy/amine mixtures during cure,[82] we have estimated the maximum change in density in our system at 7%. Clearly, this value alone cannot explain the observed increase in $\Delta\epsilon_N$ during cross-linking. Molecular simulation was then conducted (see Experimental Section) in order to investigate the variation in $\langle r^2\rangle$ during cross-linking. To cut down on the simulation time, we have conducted a series of runs on a PPO sample with molecular weight of 1194 g/mol. The value of mean-squared end-to-end distance increases by 26%, from 421 Å^2 in the unreacted mixture to 531 Å^2 in the cured network. Interestingly, an initial simulation run on a higher molecular weight PPO (MW = 4023 g/mol) yielded an identical result. In all, we established that the calculated increase in density and $\langle r^2\rangle$, taken together, still could not account for the observed increase in $\Delta\epsilon_N$ during cross-linking and that other factors must play a role. One explanation lies in the increasing cross-correlations between PPO chains, which gradually evolve during cross-linking but are not accounted for in eq 3.

We wish to mention another interesting observation. When DGEBA was replaced by an epoxy-terminated PPO380 and PPO640 (the results are not shown here), the measured increase in $\Delta\epsilon_N$ during cross-linking was much less than 150%. The calculated values were 30% and 37% for PPO380 and PPO640, respectively, suggesting that the increase in cross-correlation between PPO chains is favored by the presence of more rigid (than PPO) DGEBA spacer. This is another interesting subject for further study.

Changes in Relaxation Time during Network Formation. We next examine the change of relaxation time during cross-linking. The temperature dependence of the average relaxation time for segmental (τ_S) and normal mode (τ_N) for MPPO4000 with extent of reaction as a parameter is plotted in Figure 13. For clarity, we plot only the data at conversions of 0, 31%, and 100%. The solid lines in Figure 13 are fits to the VFT equation, and the corresponding best-fit parameters are summarized in Table 5. We stress that τ_0 for the segmental process in MPPO4000 was set at the attempt frequency (10^{-14} s) and that the same Vogel temperature was used to fit the segmental and the normal mode process. The temperature dependence of the average relaxation time for segmental (τ_S) and normal mode (τ_N) for MSPPO5000 with extent of reaction as a parameter is plotted in Figure 14. The solid lines in Figure 14 are fits to the VFT equation, and the corresponding best-fit parameters are summarized in Table 6.

It is interesting to point out that the fragility of networks does not change during cross-linking. How

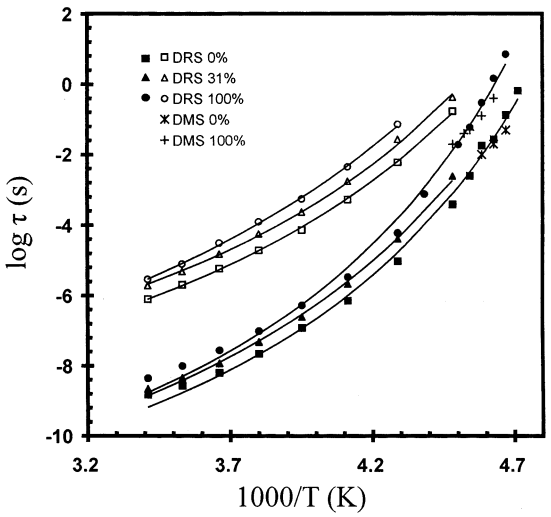

Figure 13. Average DRS relaxation time for the segmental (filleds symbols) and normal mode (open symbols) process in MPPO4000 as a function of reciprocal temperature with extent of reaction as a parameter. Data for the average DMS relaxation time for the segmental process for 0% (∗) and 100% (+) conversion are included for comparison.

Table 5. VFT Parameters for Normal and Segmental Processes in MPPO2000 and MPPO4000 during Cross-Linking

	normal mode			segmental mode		
extent of reaction	τ_0 (s)	B (K)	T_v (K)	τ_0 (s)	B (K)	T_v (K)
MPPO2000: 0%	5.8×10^{-12}	1330	165	1.0×10^{-14}	1491	165
MPPO2000: 6%	8.1×10^{-12}	1299	167	1.0×10^{-14}	1492	167
MPPO2000: 13%	2.1×10^{-11}	1221	168	1.0×10^{-14}	1510	168
MPPO2000: 23%	1.7×10^{-11}	1269	169	1.0×10^{-14}	1515	169
MPPO2000: 52%	1.7×10^{-11}	1299	172	1.0×10^{-14}	1526	172
MPPO2000: 75%	2.0×10^{-11}	1350	173	1.0×10^{-14}	1549	173
MPPO2000: 100%	3.3×10^{-12}	1584	175	1.0×10^{-14}	1606	175
MPPO4000: 0%	1.3×10^{-11}	1500	159	1.0×10^{-14}	1525	159
MPPO4000: 12%	3.3×10^{-11}	1400	163	1.0×10^{-14}	1516	163
MPPO4000: 31%	6.1×10^{-11}	1300	164	1.0×10^{-14}	1530	164
MPPO4000: 46%	6.5×10^{-11}	1400	164	1.0×10^{-14}	1554	164
MPPO4000: 64%	4.7×10^{-11}	1400	163	1.0×10^{-14}	1585	163
MPPO4000: 76%	4.8×10^{-11}	1500	163	1.0×10^{-14}	1584	163
MPPO4000: 100%	2.7×10^{-11}	1520	163	1.0×10^{-14}	1607	163

(and if) the fragility changes during cross-linking is an interesting and open question. In debating this point, an important initial consideration is the manner in which the type and concentration of dipoles vary during cure; four such scenarios were identified and exemplified in a recent publication.[25] Therefore, in describing the fragility of partially cured networks one must consider (and possibly decouple) *physical* (increased cross-link density) and *chemical* changes that accompany network formation. For example, epoxy−amine mixtures belong to the class of network formers where dipoles present in the reactants are involved in the reaction and new types of dipoles are formed. Earlier studies in the literature report a change in the fragility during cross-linking of epoxy−amine networks containing low molecular weight amines.[83] In another class of network-formers, such as vinyl-terminated poly(siloxanes) or poly(vinylethylene), where dipoles present in the reactants are not involved in the reaction, the product contains the same concentration (normalized for density changes) and type of dipolar groups. Roland[10] studied poly(vinyl ethylene) (PVE) networks and realized different cross-linked densities by adding different amounts of dicumyl peroxide to PVE. He observed an increase in the relaxation time, T_g, and fragility of the segmental

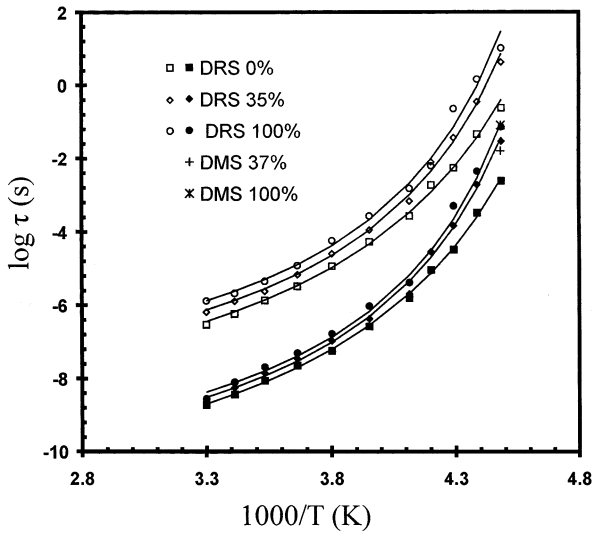

Figure 14. Average DRS relaxation time for the segmental (filleds symbols) and normal mode (open symbols) process in MSPPO5000 as a function of reciprocal temperature with extent of reaction as a parameter. Data for the average DMS relaxation time for the segmental process for 37% (+) and 100% (∗) conversion are included for comparison.

process with increasing cross-link density, suggesting that the α dynamics in the more densely cross-linked network are associated with stronger intermolecular coupling.[10,84] That led to the argument that the junctions and the chains emanating from them are effectively constraining the motions of segments well removed from the junctions. Glatz-Reichenbach et al.[14] studied another network belonging to the same class, obtained by cross-linking styrene−butyl acrylate (SB) copolymer with divinylbenzene (DVB), and speculated that the segments near the chain ends may have a different activation energy than those further away. But in two other systems, namely vinyl-terminated poly(methylphenylsiloxane),[25] PMPS, and vinyl-terminated poly(dimethylsiloxane),[22] PDMS, the fragility index was found to be independent of cross-link density, leading those authors to conclude that the distance between cross-links is greater than the length scale of the α process. Reported studies of fragility during cure of systems that contain a star polymer, however, are scarce. Randrianantoandro et al.[85] investigated a polyurethane network composed of hydroxyl-terminated three-arm PPO (MW = 720 g/mol) and hexamethylene diisocyanate (HMDI). The resulting network is termed PU720. The authors reported that the frequency at maximum dielectric loss (ω_{max}) was not affected by an increase in the degree of cross-linking over a narrow temperature range of about 10 K. More recently, Baillif et al.[86] studied a series of PU networks with varying MW of the PPO triol (MW = 6000, 700, and 260 g/mol). They reported that the fragility was independent of cross-linking for PU6000, but it varied for PU700 and PU260. We shall return to the argument about the change in fragility during cross-linking in the section below.

Although not examined in this study, the related question of the thermodynamics of networks of varying cross-link density going through T_g is of interest. Lee and McKenna[87] prepared several PPO/DGEBA networks of different cross-link density by varying the molecular weight of PPO. Following physical aging, the samples were heated; the specific heat (ΔC_p) at T_g was measured and found to be independent of the molecular weight of PPO. The implication is that there should be no change in the dynamic fragility in these systems, and this is an interesting subject for further examination.

As stated earlier in the text, the interplay of segmental and normal modes is of particular interest to us. We acknowledge reports in the literature that with decreasing temperature the α process in time-invariant systems slows down faster than the normal mode (though the two should not cross over and a theoretical explanation has been given by Ngai[88]) but hasten to add that the simultaneous effect of chemical cross-linking on τ_S and τ_N has not been systematically studied. One way to examine the effect of cross-linking on segmental and normal mode dynamics is by plotting τ_N vs τ_S with extent of reaction as a parameter. The results, shown in Figure 15, are especially revealing; the data collapse on the same line over a wide range of conversion and temperature, indicating that the course of network formation does not affect the frequency at maximum loss for the normal mode process *relative* to the segmental process. Near the glass transition, however, the temperature dependence of the segmental relaxation time is stronger than that of the normal mode, which is manifest by a slight but discernible curvature in the data in Figure 15.

Changes in Relaxation Spectrum during Network Formation. The changes in the relaxation spectra during cross-linking are also revealing. We find that the segmental and normal mode spectra become thermodielectrically complex (the unreacted mixtures are simple) following the onset of reaction and remain such until the completion of cure. Because the spectra are complex, a comparative examination of the effect of cross-linking on the spectral shape at different stages of network formation must be carried out at a temperature that bears the same relation to the T_g of each network. Figure 16 illustrates the change in the KWW β parameter during cross-linking of MPPO4000, calculated for a series of spectra swept at $T = T_{gi} + 16$ K, where T_{gi} represents the DSC glass transition of a network with degree of cross-linking equal to *i*. The inset in Figure 16 contains analogous results for MSPPO500, calculated for a series of spectra swept at $T = T_{gi} + 30$ K. A steady decrease in KWW β during cross-linking is the signature of spectral broadening. The change in the spectral shape and the unchanged distance between the average segmental and normal mode relaxation time (Figure 15), taken together, suggest that the segmental and normal mode relaxations broaden and overlap during cross-linking but *retain their identities*. We made no attempts in this work at probing the time−conversion superposition, though that could be an interesting subject for future work. The broadening of the segmental process is not a new finding (e.g., refs 89−91), but precisely why the broadening occurs is still debated. Kumar et al.[92] developed a model based on the nanoscale concentration fluctuations, predicting the broadening of the α process in polymer blends. Arguments along similar lines were set forth by Roland and Ngai, though they speak of the phenomenon generically as heterogeneous broadening.[93] Randrianantoandro's work[85] on cross-linked polyurethanes containing a PPO triol (MW = 720 g/mol) showed broadening of the segmental process with increasing cross-linking density. Baillif's investigation[86] found that the KWW β parameter decreases steadily with increasing cross-linking for

Table 6. VFT Parameters for Normal and Segmental Processes in MSPPO5000 during Cross-Linking

extent of reaction (%)	normal mode			segmental mode		
	τ_0 (s)	E_a (eV)	T_v (K)	τ_0 (s)	E_a (eV)	T_v (K)
0	5.03E−10[a]	6.67E−02	1.85E+02	2.49E−12	6.79E−02	1.85E+02
23	1.17E−09	5.94E−02	1.91E+02	4.10E−12	6.12E−02	1.91E+02
41	1.92E−09	5.63E−02	1.93E+02	7.19E−12	5.71E−02	1.93E+02
59	2.36E−09	5.52E−02	1.95E+02	9.35E−12	5.55E−02	1.95E+02
70	2.60E−09	5.66E−02	1.95E+02	1.10E−11	5.60E−02	1.95E+02
80	2.90E−09	5.46E−02	1.96E+02	1.18E−11	5.40E−02	1.96E+02
100	3.85E−09	5.42E−02	1.95E+02	1.24E−11	5.41E−02	1.95E+02

[a] Read as 5.03×10^{-10}.

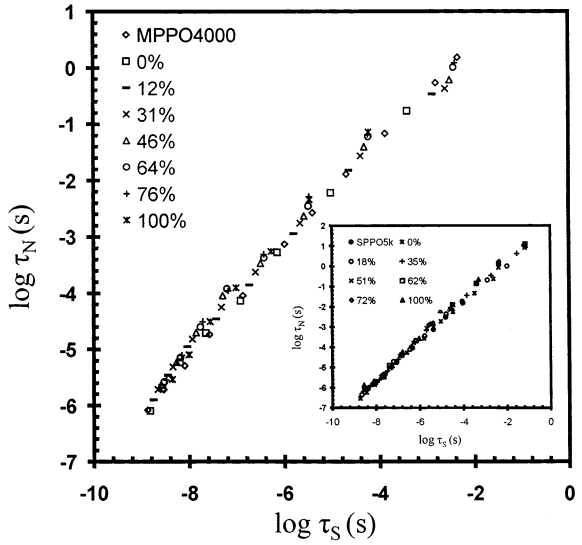

Figure 15. Normal mode relaxation time vs segmental relaxation time for MPPO4000 with extent of reaction as a parameter. Inset: analogous plot for MSPPO5000.

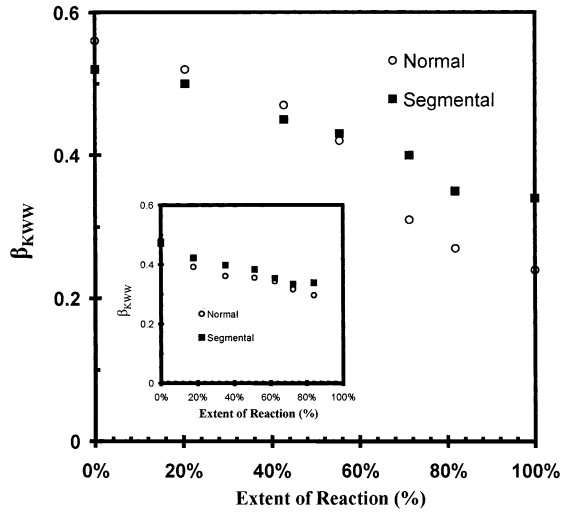

Figure 16. Normal and segmental mode β_{KWW} for MPPO4000 as a function of extent of reaction. β_{KWW} was evaluated at $T = T_{gi} + 16$ K. Inset: analogous plot for MSPPO5000 obtained at $T = T_{gi} + 30$ K.

PU6000 but goes through a minimum for PU700 and PU260. Note that the observed decrease in the KWW β parameter and the unchanged fragility with increasing cross-linking for PU6000 agree with our results. In the above-mentioned case of PMPS,[25] however, no broadening of the segmental process was observed during cross-linking. That and other segmental dynamics measures (constant fragility) led those authors to the conclusion that the distance between cross-links is greater than the length of the primitive segment and the cooperatively rearranging domain; therefore, the length scale of the α process was estimated at $l \leq 5$ nm, in agreement with a generally accepted length scale.[94] But a different picture is obtained during cross-linking of cyanate ester resins.[27] In those networks, where dipoles present in the reactants react to form nonpolar groups and where the cooperatively rearranging domain is relatively large, the α dynamics become increasingly disturbed and heterogeneous with the advancement of cross-linking, with an ultimate disappearance of the α process.

Reverting our attention to the segmental dynamics in MPPOs and MSPPOs studied in this work, we observe spectral broadening but no change in fragility during cross-linking. This is especially notable because it suggests that the concentration fluctuations that contribute to the broadening of the α spectrum may not play a crucial role in determining the fragility or the temperature dependence of the T_g-scaled relaxation time.

Dynamic Mechanical Spectroscopy during Network Formation. The results of dynamics mechanical spectroscopy (DMS) during cross-linking are described next. We preface the discussion of DMS results by a brief comment. In general, for a sequence of *n* repeat units in a type A polymer (without reversal of directional sense), the dipole vector must correlate with the displacement vector, implying a correspondence between dielectric and viscoelastic relaxations. But despite the fact that DRS and DMS results reflect the same chain motion, a direct comparison of dielectric and viscoelastic relaxation function must account for the difference in the physics that underlies the material's response to electric and mechanical fields, as argued by Watanabe.[59,60] The key point is that the calculation of G^* from ϵ^*, and vice versa, is possible only when the details of the relaxation mechanism are known. For example, for the case of pure reptation the longest relaxation time is the same for dielectric and viscoelastic correlation functions, and the normalized viscoelastic, $\mu(t)$, and dielectric, $\varphi(t)$, relaxation functions are related by $\mu(t) = \varphi(t)$, while the inclusion of dynamic tube dilation modes yields the following relation:[95] $\mu(t) = [\varphi(t)]^2$. Our systems, however, are not in the reptation regime; there is an increase in the molecular weight during network formation but no systematic increase in the length of the uninverted dipole sequence. The change in the network topology and the accompanying relaxation mechanism are complex, and hence our goal at this stage is a phenomenological comparison of the DRS and DMS dynamics.

The storage modulus (G') in the frequency domain with extent of reaction as a parameter for MPPO4000 is shown in Figure 17. The data were shifted with respect to the reference curve at 211 K. The terminal relaxation zone, characterized by the slopes of G' and

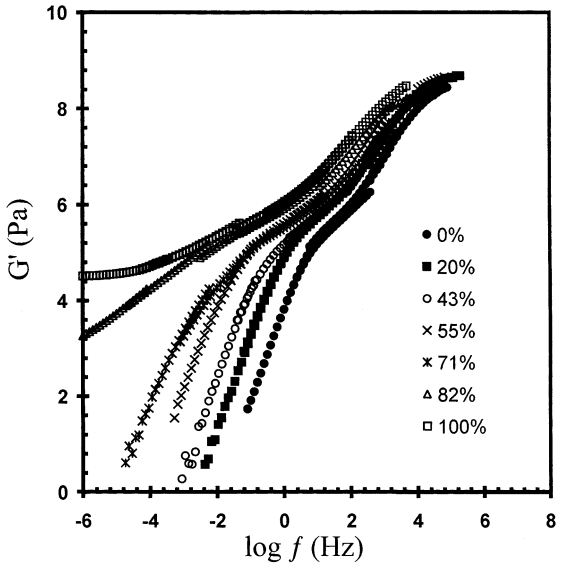

Figure 17. Storage modulus in the frequency domain with extent of reaction as a parameter for MPPO4000 at 233 K. The curves were shifted horizontally using data at 233 K as reference.

G'' vs ω of 2 and 1, respectively, was present up to 71% conversion. Deviation from the characteristic terminal relaxation response is noted in the conversion range between 71% and 82%. The DMS gel point,[96] characterized by the overlapping straight lines of G' and G'' with a slope of 0.57, was recorded at 82% conversion. This was a surprising result in that such high conversion at gel point far exceeds the prediction of Flory's gelation theory (ca. 58%).[97] Analogous results were observed for MSPPOs. Figure 18 contains master curves for storage modulus, G' (A), and loss modulus, G'' (B), in the frequency domain for MSPPO5000 with extent of reaction as a parameter, at a reference temperature of 243 K. The terminal relaxation shifts to lower frequency during network formation, and the low-frequency storage modulus attains an equilibrium value after gelation. The slopes of G' and G'' vs frequency remain at 2 and 1, respectively, up to about 50% conversion. The gel point (characterized by the overlapping straight lines of G' and G'' with a slope of 0.57, shown in Figure 19) is observed at about 55% conversion, again considerably above the prediction of Flory's gelation theory. We hasten to add, however, that similar observations were reported for other cross-linking systems;[98] the question is, what is the underlying reason in this particular case? We were especially interested in the effect of PPO molecular weight on the conversion at gel point and, to that end, have examined the kinetics and rheology of mixtures containing several lower molecular weight PPOs (MW = 280 and 400 g/mol). Interestingly enough, for both cases we observe excellent agreement between the DMS gel point and the theoretically predicted value. The implication is clear: the size of the PPO chain plays the principal role in the observed "delayed" gel point, and there are at least two reasons for that. First, the reactivity ratio, k_1/k_2, i.e., the ratio of kinetic rate constants for primary amine−epoxy (k_1) and secondary amine−epoxy (k_2) reactions, must be high. That, in turn, favors the formation of linear chains at the expense of random cross-link junctions and contributes to the delay in the onset of gelation measured by DMS. We made no attempt in this study to evaluate the kinetic rate constants but have conducted a systematic mechanistic

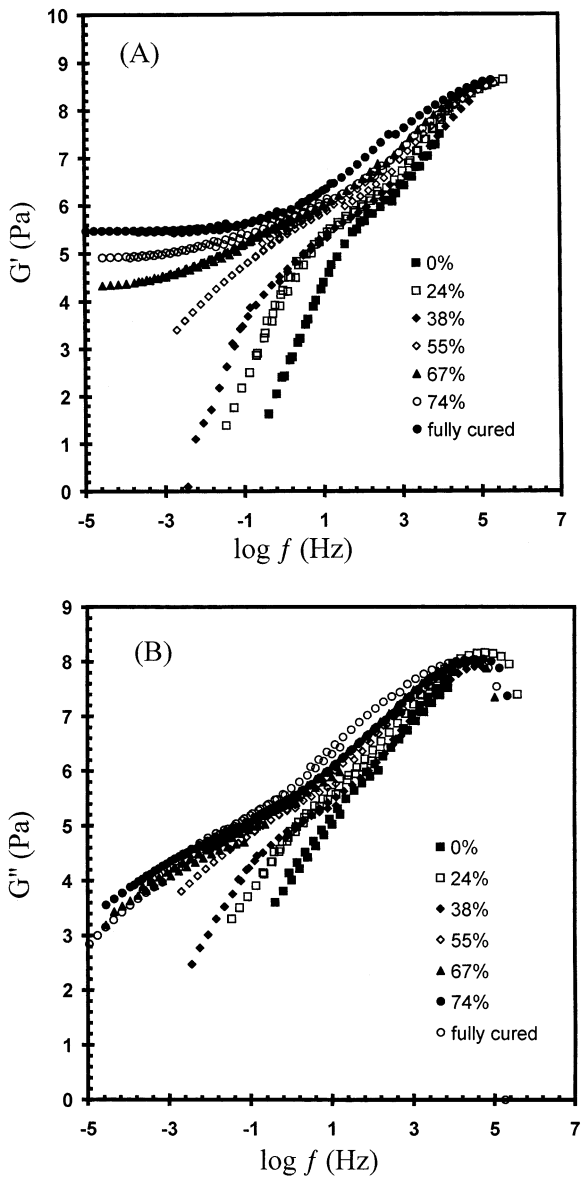

Figure 18. Storage modulus (G') and loss modulus (G'') in the frequency domain with extent of reaction as a parameter for MSPPO5000 at 233 K. The curves were shifted horizontally using data at 233 K as reference.

investigation of a series of similar systems in the past and have reported findings that support this hypothesis.[99] The second reason for the observed high conversion at gel point could be traced to the likelihood of intramolecular reactions that increases with increasing chain length.

We next describe our attempts to contrast the results of DMS and DRS, starting with the normal mode process. As stated earlier, a direct comparison of DMS and DRS data using the methodology applicable to linear chains is not appropriate here because of the different physics that underlies the change in the dielectric and viscoelastic normal modes during cross-linking. The dielectric normal mode reflects the response of the length of the chain (M_a) containing the uninverted dipole sequence, which does not change during cross-linking. The viscoelastic response, on the other hand, is sensitive to the overall molecular weight, which increases during cross-linking. The precise mechanism of the viscoelastic normal mode in our systems is not clear at present, and no further attempts at quantifying

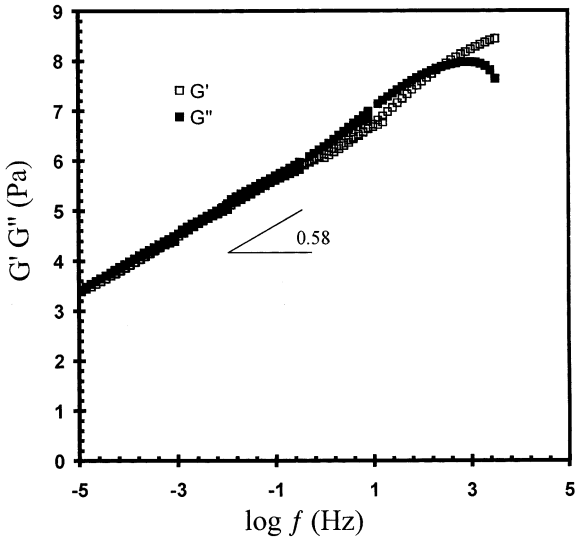

Figure 19. Storage modulus (G') and loss modulus (G'') in the frequency domain for MSPPO5000 at gel point.

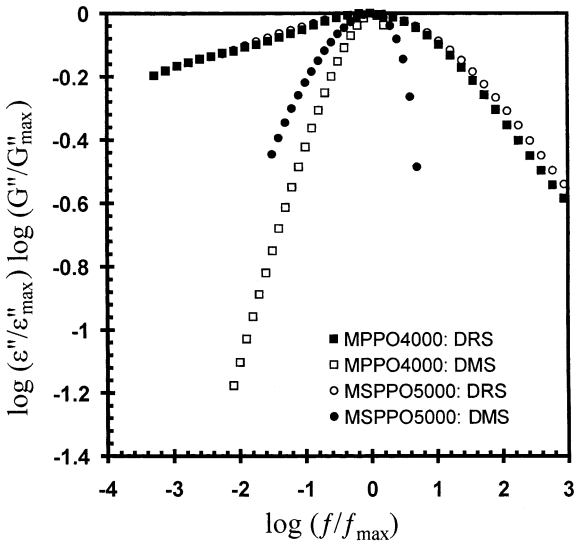

Figure 20. A comparison of normalized DRS and DMS spectra for the segmental process in fully cured MPPO4000 and MSPPO5000.

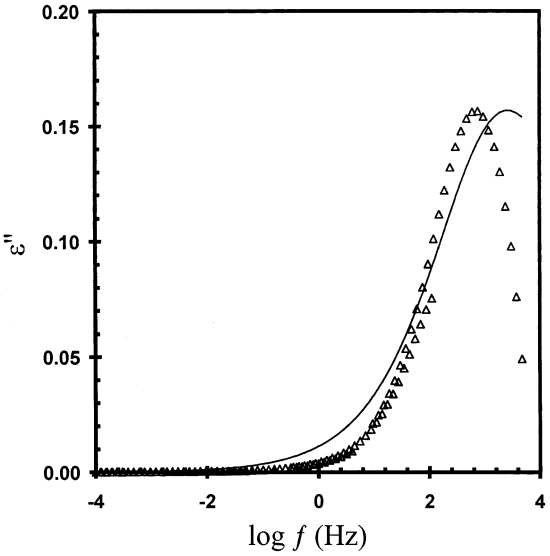

Figure 21. Dielectric loss in the frequency domain for fully cured MPPO4000 measured at 233 K. Solid lines are calculated from the HN fits and open symbols from the rheological complex modulus.

the DMS α_N dynamics were made. Recall that the observed increase in the dielectric relaxation strength for the normal mode process ($\Delta\epsilon_N$) suggests an increasing cross-correlation between PPO/SPPO chains, but further study is also needed to understand this better.

The average relaxation time for the segmental process calculated from the DMS data ($\tau_{S,DMS} = 1/\omega_{max}$) agrees very well with the DRS results for MPPOs and MSPPOs, as seen in Figures 13 and 14. Note that $\tau_{S,DMS}$ increases with increasing conversion and agrees very well with $\tau_{S,DRS}$.

A comparison of the normalized DRS and DMS spectra for the segmental process in fully cured MPPO4000 and MSPPO500 networks is illustrated in Figure 20. Despite the presence of the dielectric normal mode on the low-frequency side of the spectra, it is clear that the DRS spectra are broader that the DMS spectra. The same observation was made for the unreacted mixture.

The final attempt at a comparison of DRS and DMS data for the segmental process is made by utilizing the DiMarzio−Bishop (DB) model,[100] written as

$$\frac{\epsilon^*(\omega)}{\epsilon_0 - \epsilon_\infty} = \frac{1}{1 + KG^*(\omega)} \tag{4}$$

from which the imaginary part of dielectric constant can be expressed as

$$\epsilon'' = \Delta\epsilon_S \frac{KG''(\omega)}{[1 + KG'(\omega)]^2 + [KG''(\omega)]^2} \tag{5}$$

The dielectric relaxation strength, $\Delta\epsilon_S$, can be obtained from the HN fits as described earlier, leaving K as the only adjustable parameter. The result is presented in Figure 21 for fully cured MPPO4000; analogous observations were made at all stages of cross-linking in MPPO and MSPPO networks. The model captures the general features of the process, but the agreement with the data cannot be considered satisfactory. Solid lines are the ϵ'' value calculated from the HN fits, while the open symbols (squares and triangles) represent the ϵ'' values calculated from the rheological complex modulus. The inability of the DB model to describe such complex system is not surprising considering its inherent simplicity. Other groups have also utilized the DB model to contrast the dielectric and viscoelastic results for the segmental process in poly(butylene), PB,[101,102] and styrene-based copolymer,[103] and they reported poor agreement with the data.

Conclusions

We have completed an investigation of the interplay of segmental and normal mode dynamics in polymer networks undergoing chemical cross-linking. This work has added a new dimension to the past efforts by examining the dynamics of reactive network-forming systems where one of the components exhibits, in addition to the transverse dipole moment component ($\mu^\perp$) that gives rise to the segmental α process, a persistent cumulative dipole moment along the chain contour ($\mu^\parallel$). The two-component reactive systems were composed of (1) linear (PPO) or star (SPPO) amine-terminated poly(propylene oxide) of different molecular

weight and (2) a bifunctional epoxy prepolymer. The progress of network formation was quantitatively followed by Fourier transform near-infrared spectroscopy (NIR); the changes in the network dynamics were monitored by dielectric relaxation spectroscopy (DRS) and dynamic mechanical spectroscopy (DMS) over a wide range of frequency and temperature. The following conclusions were reached.

The dielectric relaxation strength for the segmental process ($\Delta\epsilon_S$) decreases during cure. The decrease in $\Delta\epsilon_S$ is driven primarily by the decrease in the limiting low-frequency dielectric permittivity, ϵ'_0, caused by the changes in the physical architecture (topology) of the network and the chemical nature of the contributing dipole units. (Epoxy and primary amine groups are replaced by lesser dipole strength tertiary amine and hydroxyl groups, the latter being at the origin of the local β process.) Simultaneously, the dielectric relaxation strength for the normal mode process ($\Delta\epsilon_N$) increases during cross-linking. The increase in $\Delta\epsilon_N$ was intriguing and could not be accounted for only by the increase in the network density and the mean-squared end-to-end distance. It appears that increasing cross-correlations between PPO/SPPO chains evolve gradually during cure and contribute to an increase in $\Delta\epsilon_N$. The average relaxation time for segmental (τ_S) and normal mode (τ_N) process increases in the course of network formation, but the distance between τ_S and τ_N varies little and the T_g-scaled fragility remains unchanged. There is a gradually increasing overlap between segmental and normal mode relaxations during cure, but most notably, the two processes retain their identities. The DRS spectra for segmental and normal mode become thermodielectrically complex following the onset of reactions (the unreacted mixtures are simple) and broaden in the course of cure as measured by a decreasing KWW β parameter. It is curious that the spectra broaden while the fragility remains unchanged during cross-linking. This is especially interesting because it suggests that the concentration fluctuations that contribute to the broadening of the α spectrum may not play a crucial role in determining the fragility or the temperature dependence of the T_g-scaled relaxation time. The DMS results show the characteristic segmental and terminal relaxation zones. The deviation from the characteristic terminal zone response, with the slopes of G' and G'' vs frequency of 2 and 1, respectively, is first noted at higher than expected (theoretically) conversion. The gel point in MPPO4000 and MSPPO5000, identified by the overlapping straight lines of G' and G'', was recorded at a conversion above that predicted by Flory's gelation theory. The observed "delayed" gelation is rationalized in terms of the high molecular weight of the amine-terminated PPO/SPPO, a high reactivity ratio of the kinetic rate constants for primary amine−epoxy and secondary amine−epoxy reactions, and a likelihood of intramolecular reactions. The average relaxation time for the segmental process calculated from the DMS data agrees well with the DRS results. Finally, a comparison of the normalized DRS and DMS spectra for the segmental process in MPPO and MSPPO networks was interesting. Despite the presence of the dielectric normal mode on the low-frequency side of the spectra, it is observed that the DRS spectra are broader that the DMS spectra at all stages of network formation.

Acknowledgment. This material is based on work supported by National Science Foundation under Grants DMR-0101182 and DMR-9975592. Helpful comments by Professor Radomir Kovačević are gratefully acknowledged.

References and Notes

(1) Lane, J. W.; Seferis, J. C.; Bachmann, M. A. *J. Appl. Polym. Sci.* **1986**, *31*, 1155.
(2) Nass, K. A.; Seferis, J. C. *Polym. Eng. Sci.* **1988**, *29*, 315.
(3) Senturia, S. D.; Sheppard, N. F. *Adv. Polym. Sci.* **1986**, *80*, 1.
(4) Kranbuehl, D. E.; Delos, S.; Yi, E.; Mayer, J.; Jarvie, T.; Winfree, W.; Hou, T. *Polym. Eng. Sci.* **1986**, *26*, 338.
(5) Mangion, M. B. M.; Johari, G. P. *Macromolecules* **1990**, *23*, 3687.
(6) Mangion, M. B. M.; Johari, G. P. *J. Polym. Sci., Part B: Polym. Phys.* **1991**, *29*, 1117.
(7) Mangion, M. B. M.; Johari, G. P. *J. Polym. Sci., Part B: Polym. Phys.* **1991**, *29*, 1127.
(8) Maistros, G. M.; Block, H.; Bucknall, C. B.; Partridge, I. K. *Polymer* **1992**, *33*, 4470.
(9) MacKinnon, A. J.; Jenkins, S. D.; McGrail, P. T.; Pethrick, R. A. *Macromolecules* **1992**, *25*, 3492.
(10) Roland, C. M. *Macromolecules* **1994**, *27*, 4242, 1127.
(11) Maistros, G. M.; Bucknall, C. B. *Polym. Eng. Sci.* **1994**, *34*, 1517.
(12) Deng, Y.; Martin, G. C. *Macromolecules* **1994**, *27*, 5141.
(13) Stephan, F.; Seytre, G.; Boiteux, G.; Ulanski, J. *J. Non-Cryst. Solids* **1994**, *172−4*, 1001.
(14) Glatz-Reichenback, J.; Sorriero, L.; Fitzgerald, J. *Macromolecules* **1994**, *27*, 1338.
(15) Butta, E.; Livi, A.; Levita, G.; Rolla, P. A. *J. Polym. Sci., Part B: Polym. Phys.* **1995**, *33*, 2253.
(16) Fournier, J.; Williams, G.; Duch, C.; Aldridge, G. A. *Macromolecules* **1996**, *29*, 7097.
(17) Casalini, R.; Corezzi, S, Fioretto, D.; Livi, A.; Rolla, P. A. *Chem. Phys. Lett.* **1996**, *258*, 470.
(18) Ulanski, J.; Friedrich, K.; Boiteux, G.; Seytre, G. *J. Appl. Polym. Sci.* **1997**, *65*, 1143.
(19) Wasylyshyn, D. A.; Johari, G. P.; Tombari, E.; Salvetti, G. *Chem. Phys.* **1997**, *223*, 313.
(20) Nicolai, T.; Prochazka, F.; Durand, D. *Phys. Rev. Lett.* **1999**, *82*, 863.
(21) Williams, G.; Smith, I. K.; Aldridge, G. A.; Holmes, P.; Varma, S. *Polymer* **2001**, *42*, 3533.
(22) Schroeder, M. J.; Roland, C. M. *Macromolecules* **2002**, *35*, 2676.
(23) Andjelic, S.; Fitz, B.; Mijovic, J. *Macromolecules* **1997**, *30*, 5239.
(24) Andjelic, S.; Mijović, J. *Macromolecules* **1998**, *31*, 2872.
(25) Fitz, B.; Mijović, J. *Macromolecules* **1999**, *32*, 3518.
(26) Fitz, B.; Mijović, J. *Macromolecules* **1999**, *32*, 4134.
(27) Fitz, B.; Mijović, J. *Macromolecules* **2000**, *33*, 887.
(28) Fitz, B.; Mijović, J. *J. Phys. Chem. B* **2000**, *104*, 12215.
(29) The polymer dynamics community has been using the term "normal mode" to describe the dielectric relaxation due to the global motion of type A chains. We acknowledge that Watanabe has advocated the use of the term "eigenmode" instead of "normal mode" for the relaxation of mathematically well-defined modes.
(30) Stockmayer, W. H.; Baur, M. E. *J. Am. Chem. Soc.* **1964**, *86*, 3485.
(31) Baur, M. E.; Stockmayer, W. H. *J. Chem. Phys.* **1965**, *43*, 4319.
(32) Stockmayer, W. H. *Pure Appl. Chem.* **1967**, *15*, 539.
(33) Burke, J. J.; Stockmayer, W. H. *Macromolecules* **1969**, *2*, 647.
(34) Adachi, K.; Kotaka, T. *Macromolecules* **1983**, *16*, 1936.
(35) Adachi, K.; Kotaka, T. *Macromolecules* **1985**, *18*, 295.
(36) Adachi, K.; Kotaka, T. *Macromolecules* **1987**, *20*, 2018.
(37) Adachi, K.; Kotaka, T. *Macromolecules* **1988**, *21*, 157.
(38) Ball, R. C.; McLeish, T. C. B. *Macromolecules* **1989**, *22*, 1911.
(39) Boese, D.; Kremer, F. *Macromolecules* **1990**, *23*, 829.
(40) Patel, S. S.; Takahashi, K. M. *Macromolecules* **1992**, *25*, 4382.
(41) Baysal, M. B.; Stockmayer, W. H. *Macromolecules* **1994**, *27*, 7429.
(42) Urakawa, O.; Adachi, K.; Kotaka, T.; Takemoto, Y.; Yasuda, H. *Macromolecules* **1994**, *27*, 7410.
(43) Watanabe, H.; Yamada, H, Urakawa, O. *Macromolecules* **1995**, *28*, 6443.

(44) Watanabe, H.; Urakawa, O.; Yamada, H.; Yao, M.-L. *Macromolecules* **1996**, *29*, 755.
(45) Karatasos, K.; Anastasiadis, S. H.; Floudas, G.; Fytas, G.; Pispas, S.; Hadjichristidis, N.; Pakula, T. *Macromolecules* **1996**, *29*, 1326.
(46) Floudas, G.; Paraskeva, S.; Hadjichristidis, N.; Fytas, G.; Chu, B.; Semenov, A. N. *J. Chem. Phys.* **1997**, *107*, 5502.
(47) Milner, S. T.; McLeish, T. C. B. *Macromolecules* **1997**, *30*, 2159.
(48) Nicolai, T.; Floudas, G. *Macromolecules* **1998**, *31*, 2578.
(49) McLeish, T. C. B.; Milner, S. T. *Adv. Polym. Sci.* **1999**, *145*, 195.
(50) Schroeder, M. J.; Roland, C. M. *Macromolecules* **1999**, *32*, 2000.
(51) Floudas, G.; Meramveliotaki, K.; Hadjichristidis, N. *Macromolecules* **1999**, *32*, 7496.
(52) Kyritsis, A.; Pissis, P.; Mai, S.-M.; Booth, C. *Macromolecules* **2000**, *33*, 4581.
(53) Nicolai, T. *Macromolecules* **2001**, *34*, 8995.
(54) Frischknecht, A. L.; Milner, S. T.; Pryke, A.; Young, R. N.; Hawkins, R.; McLeish, T. C. B. *Macromolecules* **2002**, *35*, 4801.
(55) Vega, D. A.; Sebastian, J. M.; Russel, W. B.; Register, R. A. *Macromolecules* **2002**, *35*, 169.
(56) Watanabe, H.; Matsumiya, Y.; Inoue, T. *Macromolecules* **2002**, *35*, 2339.
(57) Adachi, K.; Kotaka, T. *Prog. Polym. Sci.* **1993**, *18*, 585.
(58) Adachi, K. In *Dielectric Spectroscopy of Polymeric Materials*; Runt, J. P., Fitzgerald, J. J., Eds.; American Chemical Society: Washington, DC, 1997; Chapter 9, pp 261−282.
(59) Watanabe, H. *Prog. Polym. Sci.* **1999**, *24*, 1253.
(60) Watanabe, H. *Macromol. Rapid Commun.* **2001**, *22*, 127.
(61) Mijović, J.; Sun, M.; Han, Y. *Macromolecules* **2002**, *35*, 6417.
(62) Fitz, B.; Andjelic, S.; Mijovic, J. *Macromolecules* **1997**, *30*, 5227.
(63) Mijović, J.; Miura, N.; Monetta, T.; Duan, Y. *Polym. News* **2001**, *26*, 251.
(64) Mijović, J.; Andjelic, S. *Macromolecules* **1996**, *29*, 239.
(65) Mijović, J.; Zhang, H. *Macromolecules* **2003**, *36*, 1279.
(66) Williams, G. Dielectric relaxation spectroscopy of amorphous polymer systems: the modern approaches. In *Keynote Lectures in Selected Topics of Polymer Science*; Riande, E., Ed.; CSIC: Madrid, 1997; Chapter 1, pp 1−40.
(67) Williams, G. Theory of dielectric properties. In *Dielectric Spectroscopy of Polymeric Materials*; Runt, J. P., Fitzgerald, J. J., Eds.; American Chemical Society: Washington, DC, 1997; Chapter 1, pp 3−65.
(68) Kremer, F., Schonhals, A., Eds.; *Broadband Dielectric Spectroscopy*; Springer-Verlag: Berlin, 2002.
(69) Havriliak, S., Jr.; Negami, S. *Polymer* **1967**, *8*, 161.
(70) Cole, R. H.; Cole, K. S. *J. Chem. Phys.* **1942**, *10*, 98.
(71) Williams, G.; Watts, D. C. *Trans. Faraday Soc.* **1970**, *66*, 80.
(72) Casalini, R.; Livi, A.; Rolla, P.; Levita, G.; Fioretto, D. *Phys. Rev. B* **1996**, *53*, 564.
(73) Paluch, M.; Roland, C. M.; Gapinski, J.; Patkowski, A. *J. Chem. Phys.* **2003**, *118*, 3177.
(74) Angell, C. A. *J. Res. NIST* **1997**, *102*, 171.
(75) Green, J. L.; Ito, K.; Xu, K.; Angell, C. A. *J. Chem. Phys. B* **1999**, *103*, 3991.
(76) Richert, R.; Angell, C. A. *J. Phys. Chem.* **1998**, *108*, 9016.
(77) Mijović, J.; Andjelic, S. *Macromolecules* **1995**, *28*, 2787.
(78) Williams, G.; Smith, I. K.; Homes, P. A.; Varma, S. *J. Phys.: Condens. Matter* **1999**, *11*, A57.
(79) McCrum, N. G.; Read, B. E.; Williams, G. *Anelastic and Dielectric Effects in Polymeric Solids*; Dover: New York, 1991.
(80) Frohlich, H. *Theory of Dielectrics*, 2nd ed.; Oxford University Press: Oxford, UK, 1958.
(81) Le Fevre, R. J. W. *Dipole Moments: Their Measurement and Application in Chemistry*; Wiley: New York, 1953.
(82) Mijović, J.; Wang, H. T. *SAMPE J.* **1988**, *24*, 42.
(83) Mijović, J. Dielectic spectroscopy of reactive network-forming polymers. In Kremer, F., Schonhals, A., Eds.; *Broadband Dielectric Spectroscopy*; Springer-Verlag: Berlin, 2002; Chapter 9, pp 350−385.
(84) Ngai, K. L.; Roland, C. M. *Macromolecules* **1993**, *26*, 6824.
(85) Randrianantoandro, H.; Nicolai, T.; Durand, D.; Prochazka, F. *Macromolecules* **1997**, *30*, 5893.
(86) Baillif, P.; Tabellout, M.; Emery, J. R. *Polymer* **2000**, *41*, 5305.
(87) Lee, A.; McKenna, G. B. *Polymer* **1988**, *29*, 1812.
(88) Ngai, K. L. *J. Non-Cryst. Solids* **2000**, *275*, 7.
(89) Fischer, E. W.; Zetsche, A. *Polym. Prepr. (Am. Chem. Soc., Div. Polym. Chem.)* **1992**, *33*, 78.
(90) Katana, G.; Fischer, E. W.; Hack, Th.; Abetz, V.; Kremer, F. *Macromolecules* **1995**, *28*, 2714.
(91) Kamath, S.; Colby, R. H.; Kumar, S.; Karatasos, K.; Floudas, G.; Fytas, G.; Roovers, J. E. L. *J. Chem. Phys.* **1999**, *111*, 6121.
(92) Kumar, S.; Colby, R.; Anastasiadis, S.; Fytas, G. *J. Chem. Phys.* **1996**, *105*, 3777.
(93) Roland, C. M.; Ngai, K. L. *Macromolecules* **1992**, *25*, 363.
(94) Sillescu, H. *J. Non-Cryst. Solids* **1999**, *243*, 81.
(95) Matsumiya, Y.; Watanabe, H.; Osaki, K. *Macromolecules* **2000**, *33*, 499.
(96) Winter, H. H.; Mours, M. *Adv. Polym. Sci.* **1997**, *134*, 165.
(97) Flory, P. J. *Principles of Polymer Chemistry*; Cornell University Press: Ithaca, NY, 1953.
(98) Hsu, C. P.; Lee, L. J. *Polymer* **1993**, *34*, 4516.
(99) Mijović, J.; Fishbain, A.; Wijaya, J. *Macromolecules* **1992**, *25*, 979.
(100) DiMarzio, E. A.; Bishop, M. *J. Chem. Phys.* **1974**, *60*, 3802.
(101) McKenna, G. B.; Mopsik, F. I.; Zorn, R.; Richter, D. *SPE ANTEC Prepr.* **1997**, *2*, 1027.
(102) Zorn, R.; Mopsik, F. I.; McKenna, G. B.; Willner, L.; Richter, D. *J. Chem. Phys.* **1997**, *107*, 3645.
(103) Ferri, D.; Castellani, L. *Macromolecules* **2001**, *34*, 3973.

MA030072L